Proceedings of the 4th World Congress on Mechanical, Chemical, and Material Engineering (MCM'18)
Madrid, Spain – August 16 – 18, 2018
Paper No. HTFF 134
DOI: 10.11159/htff18.134

Conjugate Heat Transfer in a Solar-Driven Enhanced Thermal Energy Storage System Using PCM

J. P. Solano, F. Roig, F. Illán, R. Herrero-Martín, J. Pérez-García, A. García
Departamento de Ingeniería Térmica y de Fluidos, Universidad Politécnica de Cartagena
Campus Muralla del Mar (30202), Cartagena, Spain
juanp.solano@upct.es

Abstract **-** In this paper, a numerical analysis of the conjugate heat transfer between a heat transfer fluid, a smooth or enhanced tube and a PCM container is accomplished. The heat transfer fluid inlet and outlet boundary conditions are coupled with the solar collector that provides the fluid with thermal energy, considering the dynamics of a solar irradiance curve. This provides the model with a realistic approach that allows for quantifying the effect of a given solar irradiance curve on the capacity of thermal energy storage. The lower latent thermal storage detected in winter conditions (peak irradiance of 500 W/m^2 and 9 hours of solar light) with a standard shell and tube container can be overcome with the use of a rectangular finned tube. An increase of the heat transfer surface to PCM volume ratio of 5.7 times yields a 2.2-fold augmentation of thermal energy storage.

Keywords**:** Solar Energy, Thermal Energy Storage, PCM, CFD, Enhanced Heat Transfer.

1. Introduction

The intermittent nature of solar energy made essential the challenging development of thermal energy storage technologies. Latent heat storage (LHS) offers high storage density and a much smaller temperature change in contrast to sensible heat systems. In the LHS method, heat is stored through the phase change of a material at a relatively constant temperature. The use of phase change materials (PCM) [1] for LHS purposes presents, however, major drawbacks that have to be faced, such as long-term stability of storage properties, low thermal conductivity, phase segregation, and subcooling during the phase change process [2].

Novel designs of LHS systems have been driven lately by the the employment of numerical modelling, which has recently gained considerable attention [3]. CFD modelling strategies offer unique capabilities in terms of design feasibility [4]. Finite difference [5-6], finite volume and finite element methods [7-9] have been typically employed for modelling solidification and melting problems, in general in combination with the enthalpy method [10-12].

The low thermal conductivity of PCMs and negligible bulk motion during melting and solidification yields dominant thermal resistances in the PCM side of thermal energy storage systems, which makes compulsory the use of any enhancement technique, that are usually based on the use of extended surfaces or the random mixing of the PCM with high thermal conductivity particles such as carbon fibres and metal beads [4]. The use of metal foam matrices has been reported by Sundarram and Li [13] considered both the metal and the PCM domains and the heat exchanged between them. They used the commercial FE analysis package COMSOL. Liu et al [14] also developed a numerical model to analyse the heat transfer enhancement employing a metal foam in a shell-and-tube type LHTES during the PCM melting process. Feng et al [15] compared the numerical results obtained approaching the problem in two ways (pore-scale and volumen-averaged). Both works employed Ansys-Fluent.

According to Rathod and Banerjee [16] fin enhancement was found to be a very feasible solution due to their unique advantages such as simpler design, easier manufacturing, lower cost and higher efficiency. Regarding 3D numerical models, there is a scarce number of works published. Shatikian et al [17] carried out the transient 3D numerical study on the PCM melting in a heat sink, as the thermal storage unit, with a constant heat flux in the horizontal base using internal vertical aluminium fins. The work showed the effect of the height and the thickness of the fins on the PCM melting process. Youssef et al [4] simulated a novel PCM heat exchanger with eight spiral-wired tubes and enclosed with metal sheets. The organic PCM was charged in the outer finned tube side while the heat transfer fluid flowed through the tube side.

In this work, a 3D numerical analysis of the conjugate heat transfer between a heat transfer fluid, a smooth or enhanced tube and a PCM container is accomplished. The heat transfer fluid inlet and outlet boundary conditions are coupled with the solar collector that provides the fluid with thermal energy, considering the dynamics of a solar irradiance curve. This provides the model with a realistic approach that allows for quantifying the effect of a given solar irradiance curve on the capacity of thermal energy storage.

2. Numerical Model

The standard geometry under investigation is a concentric tube container. The heat transfer fluid flows across the inner tube, and the PCM is uniformly distributed in the shell side. The tube is made of aluminium, with an inner tube diameter of 33 mm and a wall thickness of 1 mm. A total length L=500 mm and shell side diameter 118 mm yields a PCM volume of 5 l. The enhanced design consists of a finned tube with 8 equally distributed rectangular fins of thickness t=2 mm and height H=32.5 mm. The shell diameter is slightly increased in order to equally accommodate a total volume of 5 liters. A cross section of the PCM container is depicted in Fig. 1.

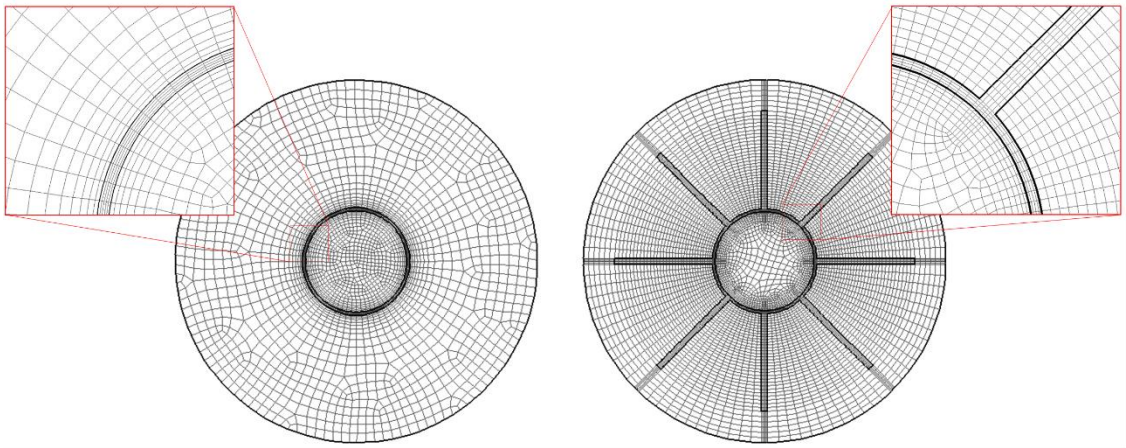

Fig. 1: Cross section of the standard (left) and enhanced (right) PCM container.

A combination of hexahedral quad and map elements is employed in both designs. The mesh is refined close to the wall in the tube side, in order to properly reproduce the entry-region and boundary layer growth effects in the inner tube. The solution of the heat conduction in the tube wall and the fins is ensured with a five-elements cross section regular mesh, as seen in the enlarged images of Fig. 1. The mesh in the shell-side increases its size progressively from the outside tube wall, where the highest temperature gradients are expected, towards the shell inner wall.

The heat transfer fluid (HTF) across the inner tube is defined as water with constant thermal properties. Uniform velocity is imposed in the tube inlet, corresponding to the normalized mass flow rate for a flat-plate solar water collector following the recommendations in [18]:

$$\dot{m}_{HTF} = 144 \, \frac{kg}{hm^2} \tag{1}$$

which, for a solar collector area A=2 m^2, yields a total mass flow rate $\dot{m}_{HTF}$=288 kg/h.

In order to define the inlet temperature, a coupling of the thermal energy storage system with the solar collector is required. In fact, the dynamics of melting are strongly dependent on the heating source. Typical models consider a constant inlet temperature or a time-dependent temperature that is not fed back by the physical connection between the PCM container and the solar collector. In this work, the transient coupling of the irradiance-based solar collector performance and the conjugate heat transfer between the heat transfer fluid is modelled, following the sketch of Fig. 2:

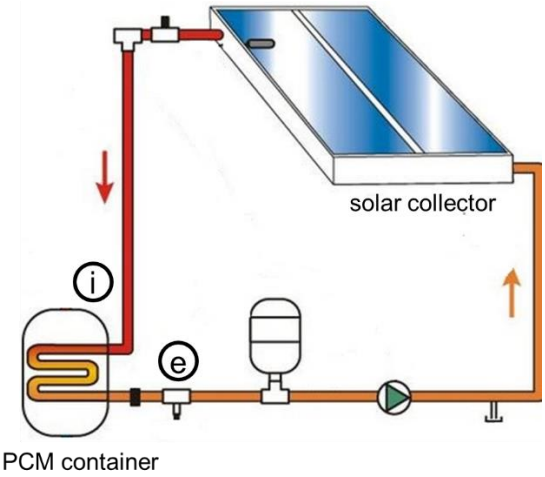

Fig. 2: Sketch for the coupling of the PCM container and the solar collector dynamic performance.

The inlet temperature T_i is defined at every time step as:

$$T_i^{n+1} = T_e^n + \frac{G^n A \eta}{\dot{m} c_p} \tag{2}$$

where G is the solar irradiance and η is the efficiency of the solar collector. In the present investigation, two opposite scenarios corresponding to winter and summer are considered:

$$G_{winter}(t) = 250\left[1 - cos\left(\frac{\pi t}{16200}\right)\right] \tag{3}$$

$$G_{summer}(t) = 500\left[1 - cos\left(\frac{\pi t}{27000}\right)\right] \tag{4}$$

The efficiency of the flat plate solar collector is given in [19]:

$$\eta = 0{,}77 - 5{,}76 \cdot T^* \tag{5}$$

where $T^* = (T_{HTF} - T_{amb})/G$. In real conditions, the expected temperature increase of the heat transfer fluid during an operating cycle would yield a viscosity decrease and a consequent increase in the Reynolds number, if mass flow is kept constant. The influence of the increased tube-side heat transfer coefficient on the conjugate heat transfer towards the PCM is, however, considered negligible as the dominant thermal resistance appears in the shell side. Following this reasoning, an initial solution of the tube flow is obtained by the integration of continuity and momentum equations:

$$\nabla \cdot \mathbf{u} = \mathbf{0} \tag{6}$$

$$\rho \mathbf{u} \cdot \nabla \mathbf{u} = -\nabla p \tag{7}$$

Once the solution of the tube flow is obtained, the melting and solidification model is activated, and the solution of equations (6) and (7) is cancelled, for sake of reduced computational cost. The energy equation in unsteady conditions (8) is integrated over the ensemble heat transfer fluid – tube – PCM, where the decoupled, steady-state velocity field **u** obtained with (6) and (7) is imposed over the applicable fluid domains:

$$\frac{\partial}{\partial t}(\rho H) + \Delta \cdot (\rho \boldsymbol{u} H) = \nabla \cdot (k \Delta T) \quad (8)$$

In the equations above, **u** is the velocity vector, p is the pressure, T is the temperature and H is the enthalpy of the pCM. As initial condition for the unsteady energy problem, a uniform temperature T=298 K (summer) or T=288 K (winter) is imposed over the whole domain. The progressive increase of the inlet fluid temperature, according to the irradiance dynamics involved in Eq. (2), drive the thermal energy storage in the PCM container.

Table 1 summarizes the thermal properties of the water, aluminium and paraffin wax considered in this work as PCM:

Table 1: Thermal properties of the materials.

	ρ (kg/m^3)	μ (kg/m·s)	c_p (J/kg·K)	k (W/m·K)	λ (J/kg)	$T_{solidus}$ (K)	$T_{liquidus}$ (K)
water	998.2	0.001003	4182	0.6	-	-	-
aluminium	2719	-	871	202.4	-	-	-
paraffin wax	750	0.003833	3100	0.15	166000	321.7	328.6

3. Results

An initial set of simulations were obtained for the standard PCM container in winter (Eq. 3) and summer (Eq. 4) conditions. The aim of this approach is to describe the influence of the solar irradiance curves on the melting capacity of the system, when a solar collector with area A=2 m^2 and efficiency given by Eq (5) is used. In winter, a total number of 9 h of solar irradiance are considered, with a peak irradiance of 500 W/m^2. Conversely, 15 h of solar irradiance are defined in the summer curve, with a peak of 1000 W/m^2 (see Fig. 3a). The heat transfer fluid temperature exceeds the PCM liquidus temperature between 2.5 and 4 hours after sunrise, depending on the operating conditions. This threshold dictates the start of melting, which is subsequently identified by the positive values of liquid fraction detected in Fig. 3d. As solar irradiance increases, the heat transfer fluid temperature increases, reaching its maximum value when the peak irradiance impacts on the collector. This temperature can be as high as 155 °C in summer, which shows the importance of the heat transfer design to accommodate lower temperatures in the PCM container. The thermal efficiency of the collector also decreases abruptly when both solar irradiance levels and HTF temperature are high. Noticeably, the ensemble is unable to melt all the paraffin wax in winter conditions, whereas full liquid PCM is obtained in summer soon after noon. The instantaneous heat absorbed by the PCM container (Fig 3e) follows an irradiance-shaped curve, affected by the changes in the thermal efficiency of the collector and the different heat transfer rates associated to the phase change of the PCM. As depicted in Fig 3f, the thermal energy storage in summer exceeds by 2.6-fold the results obtained in winter.

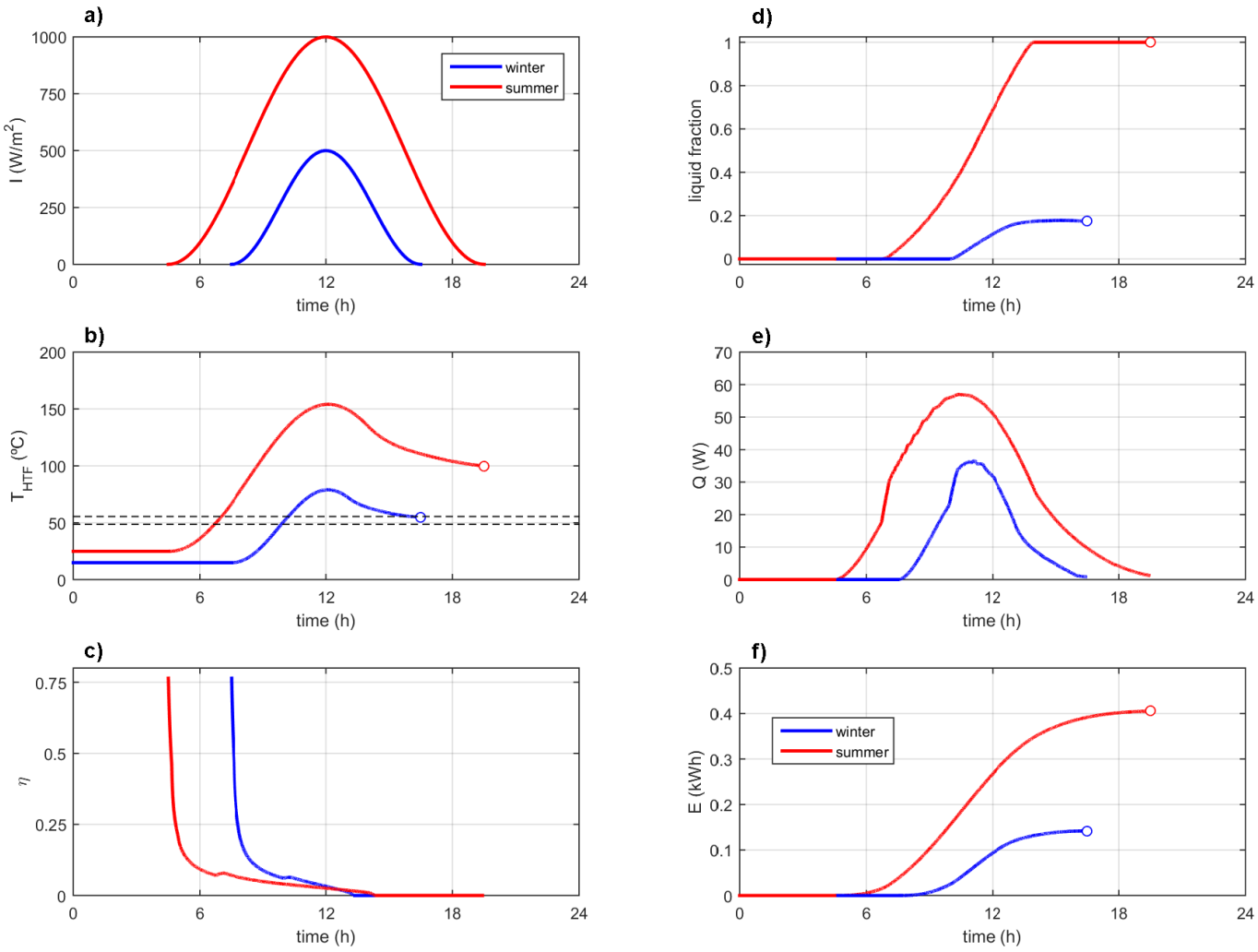

Fig. 3: Performance of the smooth-tube accumulator in winter and summer conditions.

Owing to the low thermal conductivity of the paraffin wax and the absence of significant bulk motion during the melting, the only effective technique for enhancing heat transfer is the augmentation of the heat transfer surface. In this paper, eight equally distributed rectangular fins are proposed, as explained in section 2. The ratio between the heat transfer surface and the PCM volume extends from 11 m^2/m^3 in the standard configuration to 63 m^2/m^3 in the finned geometry. The impact of the fins on the dissipation of heat is shown in Fig. 4, which presents the temperature distribution in the cross section of the PCM container 2h15m after winter sunrise. Even though the temperatures reached are still well below the liquidus temperature of the paraffin wax, the impact on melting can be observed in Fig. 5, where the liquid fraction for the standard and enhanced geometries at four equally distributed instants of the solar irradiance curved is shown. While a vast majority of the PCM is melted at winter noon ($t/\tau=0.5$) for the enhanced container, only a small fraction of the PCM is liquid in the smooth tube configuration.

The characteristics of the process can be analysed in more detail in Fig. 6, where it is noticeable how the smooth tube configuration yields higher peak heat transfer fluid temperatures than the enhanced design. This also points out the importance of a high surface-to-volume ratio to control the temperature of the heat transfer fluid. The lower heat transfer fluid temperature also drives a higher thermal efficiency of the solar collector, which in turn increases the capacity for thermal energy storage. An augmentation of the surface-to-volume ratio of 5.7 times yields a 2.2-fold increase of thermal energy storage.

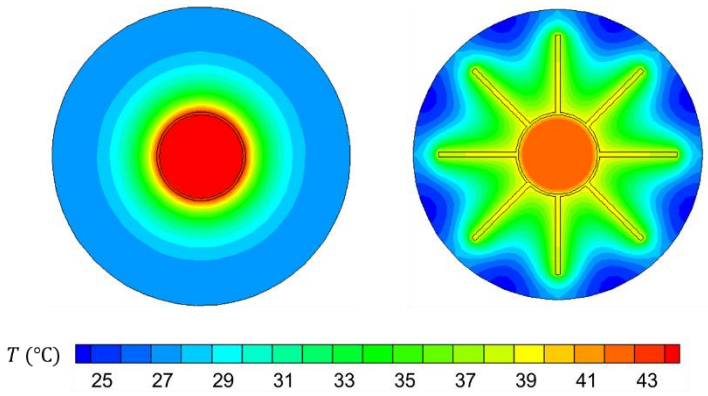

Fig. 4: Temperature field in the cross-section of the PCM accumulator in winter conditions, 2h15m after sunrise.

Although it is not shown here for sake of simplicity, the performance of the enhanced PCM container in summer conditions will bring to a fully melted PCM a few hours after sunrise, losing opportunity for further latent heat storage. This fact highlights that the different performance in winter and summer conditions might yield to a poor efficiency of the system if either low or high irradiances exist. A modularization of the overall system is recommended in order to cope with this problem, insufficiently tackled in the open literature.

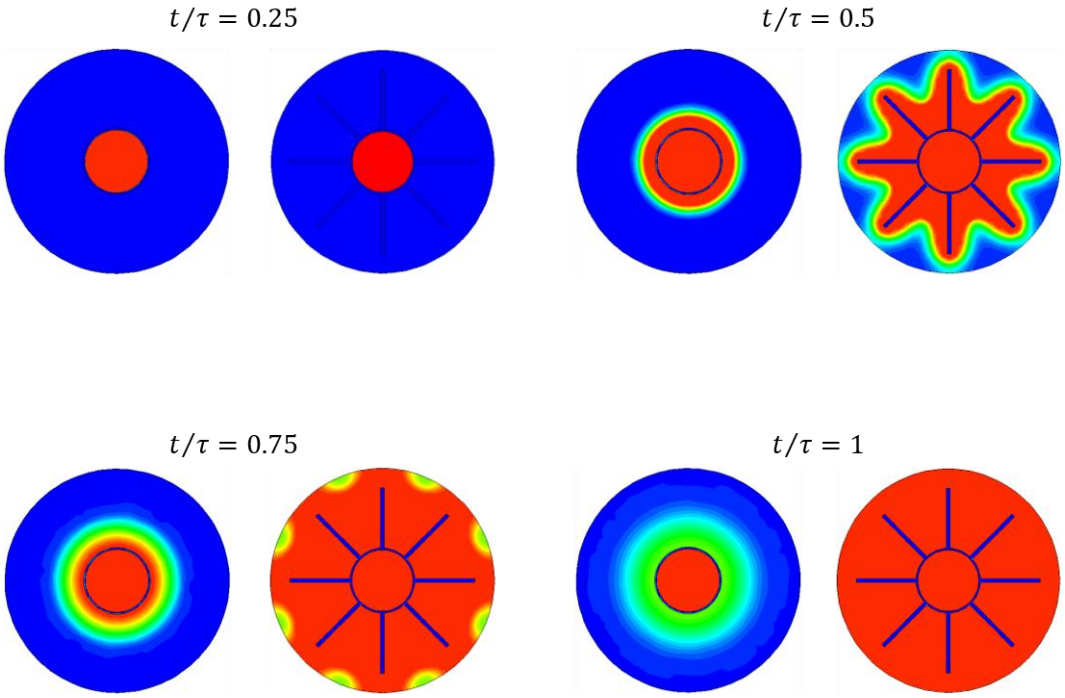

Fig. 5: Liquid fraction distribution in the regular and enhanced accumulators.

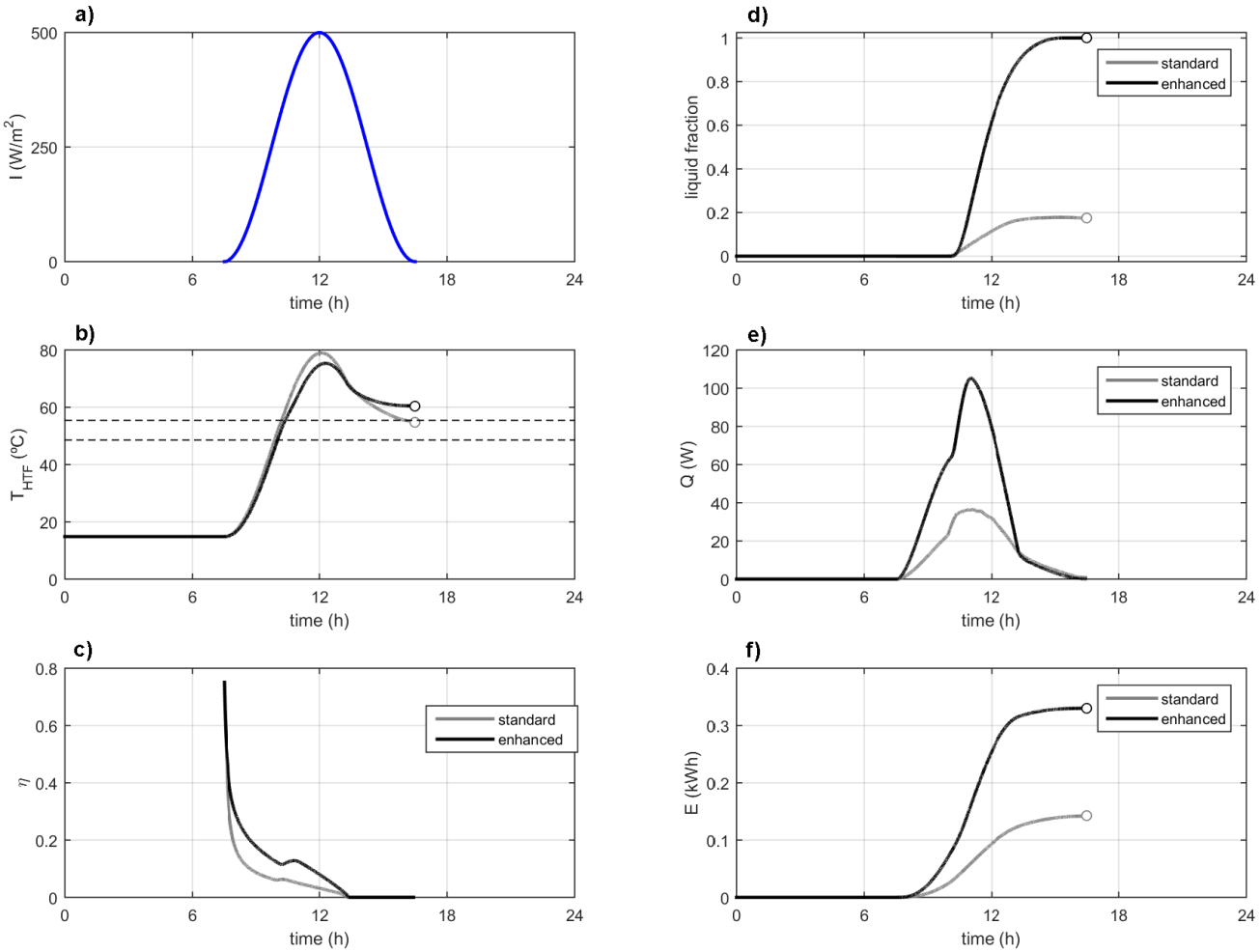

Fig. 6: Performance of regular and enhanced accumulators in winter conditions.

4. Conclusions

The coupling of the PCM charging process with the irradiance-driven dynamics of a solar collector allows for obtaining realistic transient results for solar latent thermal energy storage.

The low-intensity irradiance curves in winter conditions might lessen the capacity of a given PCM container and solar collector for thermal energy storage.

The use of extended surfaces in the PCM side improves the capacity for thermal energy storage. An augmentation of the surface-to-volume ratio of 5.7 times yields a 2.2-fold increase of thermal energy storage.

Acknowledgements

The authors gratefully acknowledge the Agencia Estatal de Investigación (MINECO, Spain) for the financial support of the ERANet-LAC project ACCUSOL: "Elaboration of the novel cooling/heating system of buildings with the application of photovoltaic cells, solar collectors and heat accumulators", Ref. PCIN-2017-059. Special thanks to Mr. Luis P. García-González from SAIT (UPCT) for easing the access to the computing cluster.

References

[1] B. Sørensen, *Solar Energy Storage*, 1st ed. 2015 ISBN: 9780124095496.

[2] M. M. Farid, A. M. Khudhair, S. A. K.Razack, S. Al-Hallaj, "A review on phase change energy storage: materials and applications," *Energy Convers. Manag*, vol. 45, pp. 1597–1615, 2004. https://doi.org/10.1016/j.enconman.2003.09.015.

[3] I. Dincer, M. A. Rosen, *Thermal Energy Storage: Systems and Applications,* 2nd ed. 2011, ISBN: 978-1-119-95662-4 Ed. Wiley.
[4] W. Youssef, Y. T. Ge, S. A. Tassou, "CFD modelling development and experimental validation of a phase change material (PCM) heat exchanger with spiral-wired tubes," *Energy Conversion and Management*, vol. 157, pp. 498-510, 2018. https://doi.org/10.1016/j.enconman.2017.12.036.
[5] P. Gimenez-Gavarrell, S. Fereres, "Glass encapsulated phase change materials for high temperature thermal energy storage," *Renew. Energy*, vol. 107, pp. 497-507, 2017.
[6] K. A. R. Ismail, R. I. R. Moraes, "A numerical and experimental investigation of different containers and PCM options for cold storage modular units for domestic applications," *Int. J. Heat Mass Transf*., vol. 52, no. 19-20, pp. 4195-4202, 2009.
[7] S. Mat, A. Abduljalil Al-Abidi, K. Sopian, M. Y. Sulaiman, T. Mohammad Abdulrahman, "Enhance heat transfer for PCM melting in triplex tube with internaleexternal fins," *Energy Convers. Manag*., vol. 74, pp. 223-236, 2013.
[8] M. Dhar, N. Barman, S. Mandal, H. Chattopadhyay, "Remelting and interface dynamics during solidification of a eutectic solution in a top-cooled rectangular cavity: a numerical study," *Int. J. Heat Mass Transf*., vol. 77, pp. 730-737, 2014.
[9] M. Chaabane, H. Mhiri, P. Bournot, "Thermal performance of an integrated collector storage solar water heater (ICSSWH) with phase change materials (PCM)," *Energy Convers. Manag*., vol. 78, pp. 897-903, 2014.
[10] M. F. Bonadies, S. Ho, J. S. Kapat, "Numerical, Analytical, Simulation of a thermal storage unit for building hot water," *Am. Inst. Aeronaut. Astronaut*., 2010.
[11] A. H. Mosaffa, F. Talati, M. A. Rosen, H. Tabrizi, Basirat, "Approximate analytical model for PCM solidification in a rectangular finned container with convective cooling boundaries," *Int. Commun. Heat Mass Transf*., vol. 39, no. 2, pp. 318-324, 2012.
[12] K. Bhagat, Saha, K. Sandip, "Numerical analysis of latent heat thermal energy storage using encapsulated phase change material for solar thermal power plant," *Renew. Energy*, vol. 95, pp. 323-336, 2016.
[13] S. S. Sundarram, and W. Li, "The effect of pore size and porosity on thermal management performance of phase change material infiltrated microcellular metal foams," *Applied Thermal Engineering*, vol. 64, pp. 147-154, 2014. http://dx.doi.org/10.1016/j.applthermaleng.2013.11.072.
[14] Z. Liu, Y. Yao, and H. Wu, "Numerical modelling for solid–liquid phase change phenomena in porous media: Shell-and-tube type latent heat thermal energy storage," *Applied Energy*, vol. 112, pp. 1222-1232, 2013.
[15] S. Feng, M. Shi, Y. Li, and T.J. Lu, "Pore-scale and volume-averaged numerical simulations of melting phase change heat transfer in finned metal foam," *International Journal of Heat and Mass Transfer*, vol. 90, pp. 838–847, 2015. http://dx.doi.org/10.1016/j.ijheatmasstransfer.2015.06.088.
[16] M. K. Rathod, J. Banerjee, "Numerical investigation on latent heat storage unit of different configurations," *Int J Mech Aerospace, Ind Mechatron Manuf Eng*, vol. 5, pp. 652–557, 2011.
[17] V. Shatikian, G. Ziskind, R. Letan, "Numerical investigation of a PCM-based heat sink with internal fins," *Int. J. Heat Mass Transf.*, vol. 48, no. 17, pp. 3689-3706, 2005.
[18] Documento Básico Ahorro de Energía, "Sección HE4–Contribución solar mínima de agua caliente sanitaria." *Código Técnico de la Edificación (CTE)*, 2013.
[19] A. García, R. Herrero-Martín and J. Pérez-García, "Experimental study of heat transfer enhancement in a flat-plate solar water collector with wire-coil inserts," *Applied Thermal Engineering*, vol. 61 no. 2, pp. 461-468, 2013.